Journal of Power Sources 196 (2011) 4264–4269

Contents lists available at ScienceDirect

Journal of Power Sources

journal homepage: www.elsevier.com/locate/jpowsour

Non-dimensional analysis of PEM fuel cell phenomena by means of AC impedance measurements

Alfredo Iranzo[a,*], Miguel Muñoz[b], Fco. Javier Pino[a], Felipe Rosa[a]

[a] Thermal Engineering Group, Energy Engineering Department, School of Engineering, Camino de los Descubrimientos s/n, 41092 Sevilla, Spain
[b] INTA – National Institute for Aerospace Technology, Ctra. San Juan del Puerto-Matalascañas, km. 33, 21130 Mazagón, Huelva, Spain

ARTICLE INFO

Article history:
Received 3 July 2010
Received in revised form 18 October 2010
Accepted 2 November 2010
Available online 9 November 2010

Keywords:
PEMFC
AC impedance
Charge transfer resistance
Bode plot
Characteristic time scale
Damkhöler

ABSTRACT

AC impedance or electrochemical impedance spectroscopy (EIS) is becoming a fundamental technique used by researchers and scientists in proton exchange membrane (PEM) fuel cell analysis and development. In this work, in situ impedance measurements are presented for a series of operating conditions in a 50 cm^2 fuel cell. The electrode charge transfer resistance was determined from the corresponding arcs of the Nyquist diagrams. The analyses were performed for H_2/O_2 and H_2/air operation at different stoichiometric factors and reactant gases humidification. Characteristic time scales of charge transfer processes at the different operating conditions were estimated from the corresponding Bode plots. These values were used for a non-dimensional analysis of the different fuel cell electrochemical and transport processes, namely electrochemical reaction versus GDL reactant transport. Fuel cell adapted Damkhöler numbers are thus presented, where the results indicate that the GDL diffusion transport is the limiting process for the cases under analysis, especially when air is used as oxidant. Additional analysis of channel convective mass transport versus GDL diffusive mass transport is also presented.

1. Introduction

AC impedance (electrochemical impedance spectroscopy) is an experimental technique widely used in the analysis of electrochemical systems, and has been established as a fundamental diagnostic and research tool for PEM fuel cells during the last years [1,2]. One of the main advantages of AC impedance techniques is that it allows for the determination of the different resistances occurring in a PEM fuel cell, corresponding to the different electrochemical and transport processes: activation or charge transfer resistance, ohmic resistance, and transport or concentration resistance. On contrast, the polarization curve itself does not provide detailed information about the different processes as they are tightly coupled and the polarization curve describes only the integral output of all processes. AC impedance is widely applied to multiple MEA analysis such as influences of the catalyst loading, PTFE content, Nafion content, GDL structure, manufacturing methods, membrane thickness, and others [1]. In an important number of studies EIS analysis has been applied to characterize fuel cell processes. Parthasarathy et al. [3], Antoine et al. [4] and Neyerlin et al. [5] analysed the oxygen reduction reaction (ORR) kinetics. Xu et al. [6] and Neyerlin et al. [7] also analysed the effect of relative humidity conditions on the ORR kinetics of PEM fuel cells. HOR (hydrogen oxidation reaction) kinetics and the effect of CO poisoning were studied by Wagner and Gülzow [8]. Transport losses were analysed by Springer et al. [9], Eikerling and Kornyshev [10], Lefebvre et al. [11], and Saab et al. [12,13], who also analysed the influence of the processing conditions of the electrode. Liu et al. [14] also studied the resistance to the protonic conduction at the cathode ionomer layer using AC impedance. The cell ohmic resistance is also commonly determined by means of AC impedance, as in the work of Cooper and Smith [15]. Romero-Castañón et al. [16], Song et al. [17] or Wagner [18] have applied AC impedance for the evaluation and optimization of the membrane electrode assembly (MEA). Additional applications are the analysis of electrode and GDL flooding or membrane dry-out, what is commonly referred to as MEA State-of-Health (SOH), as in the work reported by Fouquet et al. [19] or Mérida et al. [20]. The results are presented for the stack under analysis, but the analysis of single cells in a stack is also feasible as reported by Hakenjos et al. [21], who presented a measurement set-up featuring a multichannel frequency response analyser (FRA) for the simultaneous measurement of impedance spectra of single cells in a fuel cell stack.

Non-dimensional analysis has proven to be a powerful tool for engineering design and analysis, especially in the chemical engineering field, although its application to complex systems such as fuel cells is not yet fully established [22]. However, there is a need for comprehensive and numerically less expensive description of cell performance in order to implement it into full stack models

* Corresponding author. Tel.: +34 954487471; fax: +34 954487247.
E-mail address: aip@esi.us.es (A. Iranzo).

0378-7753/$ – see front matter © 2010 Elsevier B.V. All rights reserved.
doi:10.1016/j.jpowsour.2010.11.004

Nomenclature

a	specific catalyst surface area ($m^2\ m^{-3}$)
d	channel depth (m)
D_0	diffusion coefficient ($m^2\ s^{-1}$)
Da_{PEMFC}	Damkhöler number
F	Faraday constant (96,485 As mol^{-1})
f_{peak}	frequency (Hz)
h	mass transfer coefficient ($m\ s^{-1}$)
HFR	high frequency resistance (Ω)
I	current intensity (A)
J	diffusive flux ($kg\ m^{-2}\ s^{-1}$)
L	channel total length (m)
M_w	molecular weight ($g\ mol^{-1}$)
P	pressure (Pa)
Q_v	volume flow ($ml_N\ min^{-1}$)
R	bulk resistance (Ω)
R_c	contact resistance (Ω)
R_{cat}	cathode exchange current density ($A\ m^{-3}$)
S_{O_2}	oxygen consumption ($kg\ m^{-3}\ s^{-1}$)
Sh	Sherwood number
T	temperature (K)
V	flow velocity ($m\ s^{-1}$)
y	mass fraction

Greek symbols

δ_{GDL}	GDL thickness (m)
ε	porosity
ρ	density ($kg\ m^{-3}$)
τ	characteristic time scale (s)
λ	stoichiometric factor

Subscripts

0	reference state
BP	bipolar plate
ch	channel
chMT	channel convective mass transfer
chrt	flow residence time
diff	diffusion
EC	electrochemical
eff	effective
GDL	gas diffusion layer
MEA	membrane electrode assembly
MT	mass transfer
S	catalyst surface

that cannot be analysed by means of Computational Fluid Dynamics (CFD) models except for small-scale units [23]. Therefore, a detailed description based on dimensional analysis of the cell phenomena would be of high relevance for further stack research and development, and important contributions are already in progress as established in the work of Gyenge [22].

This work presents AC impedance results for a 50 cm^2 PEM fuel cell. The electrode activity and membrane protonic conductivity were determined elsewhere [24] based on the measurements performed for different operating conditions, aimed at the fuel cell parameter estimation needed for numerical CFD simulations [25]. In this work, the application of AC impedance measurements to the non-dimensional analysis of PEM fuel cell phenomena is presented, and results for a 50 cm^2 PEM fuel cell are reported. In particular, Nyquist and Bode plots are presented for a fuel cell with serpentine flow field, operating with oxygen and air at different humidification conditions. Measurements at several current densities are presented in order to better assess the influence of the current density on the limiting processes affecting the performance of the cell.

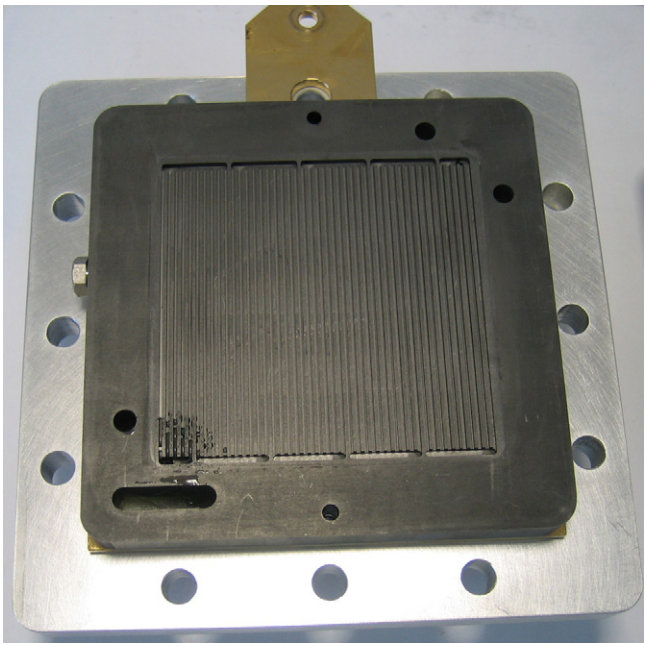

Fig. 1. Serpentine bipolar plate used in the analysis.

2. Cell description, operating conditions and experimental analysis

2.1. PEM single cell description

The single fuel cell analysed consists of commercial graphite bipolar plates with a five-channel serpentine flow field design (Fig. 1) from ElectroChem Inc. (USA). The GDL is a Sigracet 10 CC from SGL Group (Germany), with 420 μm thickness, porosity 0.82 and 10% PTFE content, featuring a micro porous layer (MPL). The 50 cm^2 membrane used is a CCM type (catalyst coated membrane) from Baltic fuel cells (Germany), with Nafion-117 and 0.3 mg Pt/cm^2 and 0.6 mg Pt/cm^2 catalyst load in anode and cathode respectively. The ratio of ionomer/carbon (I/C ratio) is 1.2/2, with 70% Pt over carbon, and a ratio ionomer/catalyst = 1/4.

2.2. Operating conditions

The operating conditions used in the analysis are listed in Table 1. Cell temperature and pressure were maintained constant during all the analysis at 60 °C and 4 bar (absolute), which are the operating conditions recommended by the cell supplier.

2.3. Experimental analysis

The experimental work was conducted in a FuelCon CT-1000 (Germany) test station, located at INTA facilities. The experimental methods and procedures were carried out following the details described in the FCTESTNET documents for single cells [26], where

Table 1
Operating conditions used for the experimental analysis.

λ_a	RH_a (%)	λ_c	RH_c (%)	Oxidant
1.5	60	5.0	60	Air
1.5	100	5.0	100	Air
2.0	100	10.0	100	Oxygen

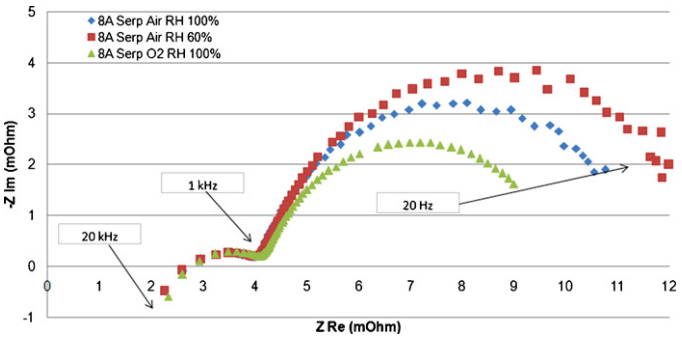

Fig. 2. Nyquist diagrams for the operation at 160 mA cm^{-2}.

its particular application to the case analysed is described in [24]. AC impedance measurements were conducted in a frequency range 20 Hz to 20 kHz on the FuelCon test station using its own frequency response analyzer (FRA). The AC impedance measurements were conducted in galvanostatic mode, where the measurements are performed by applying an AC current perturbation to the cell and measuring the potential response of the cell.

It must be mentioned that no measurements were carried out in the low frequency range (0.1–10 Hz), although such experimental work would be needed in order to obtain further information about the mass transport phenomena, and also to provide the necessary results for the validation of the non-dimensional analysis presented in Section 4. This will be accomplished in the next stage of the investigation.

3. Results

The results of the measurements are presented in the Nyquist diagrams shown in Figs. 2 and 3. The diagrams feature two impedance arcs. The Z_{Re} axis intercept at high frequencies represents the overall resistance of the cell (electronic at the bulk materials, electronic contact resistances, and ionic resistances at the membrane) and it corresponds to the high frequency resistance (HFR). In general, the next semicircle diameter at medium frequencies represents the activation overpotential losses, and the diameter of the third semicircle (at low frequencies) represents the concentration losses. However, the low frequency semicircle is typically missing in cells operating with pure oxygen [9] as is the case represented in Figs. 2 and 3. Moreover, the measurements were not conducted until the low frequencies at which this semicircle would occur, as the lowest frequency reported in Figs. 2 and 3 was 20 Hz, while concentration losses shall be measured in the range 0.1–10 Hz. Therefore, the two semicircles observed in the Nyquist plots in Figs. 2 and 3 are associated to the charge transfer resistance or activation polarization. The arc in the left of the diagram corresponds to the anode charge transfer process and the arc in the right of the diagram corresponds to the cathode charge transfer process. Although in most cases both arcs overlap themselves featuring a unique arc, the results obtained show two separate arcs of appreciably different sizes. This indicate that the anode charge transfer resistance is much smaller than the cathode resistance but still significant, probably due to the lower anode catalyst loading. None of the arcs is representing the concentration polarization losses or mass transport resistance (the reduction of the surface concentration of oxygen, mainly caused by limitations in the gas diffusion and pore blockage by liquid-phase accumulation at high current densities [27]). This specific resistance would correspond to AC frequencies below 10 Hz, and measurements were performed in the range 20 Hz to 20 kHz.

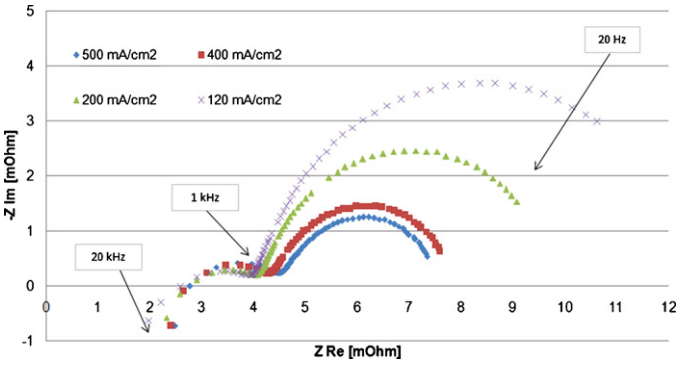

Fig. 3. Nyquist diagrams for the operation with H_2/O_2 and full humidification.

Fig. 3 shows the dependence of the charge transfer resistance at different current densities for the operation with oxygen. It is clearly observed that the diameter of the semicircle associated to the cathodic charge transfer resistance dramatically decreases as the current density increases, thus indicating that at low current densities the cathode activation losses are dominating the cell voltage loss. The reaction rate determining the cell performance is the kinetics of the oxygen reduction reaction (ORR) at the cathode, and thus the charge transfer resistance is determined by the radius of the corresponding impedance arc. The relation between the charge transfer resistance or activation polarization and the electrode overpotential is given by the Tafel equation. As current density increases the cathode overpotential decreases, as there is more energy available for the electrochemical reaction to occur. For all cases a significantly larger resistance is observed for the cathode rather than for the anode, especially at low current densities, as corresponds with the slower kinetics of the ORR. The reason for the exponential decay in the activation region of the polarization curve is clearly observed in Fig. 3, where the influence of the current density over the cathode activity is shown. Setting the current density from 120 mA cm^{-2} to 200 mA cm^{-2} results in a much larger electrode resistance reduction (50%) than changing the current density from 400 mA cm^{-2} to 500 mA cm^{-2} (6%).

As discussed, the electrode activity is determined from the corresponding arc. Fig. 2 shows the dependence of the cathode charge transfer resistance on the reactant concentration and humidification, where a minor charge transfer resistance is observed for the operation with pure oxygen. When air is used as reactant, an enhanced humidification increases the electrode activity, which was also reported by Xu et al. [6] and Neyerlin et al. [7].

The total ohmic resistivity of the cell (bulk electric resistance, electric contact resistance and protonic resistance in the membrane) is determined in the Nyquist diagram as the Z_{Re} value at $Z_{Im} = 0$ [27,28]. This value is commonly known as high frequency resistance (HFR) as it is obtained at high AC frequencies. However, a single measurement at 1 kHz, which is sometimes found as a recommendation in the literature for the determination of HFR, is not correct as observed in Figs. 2 and 3. $Z_{Im} = 0$ is obtained at different frequencies always higher than 1 kHz for the cell under analysis, and the spectra show that at 1 kHz the impedance is not purely resistive, presenting a non-zero imaginary component.

As the bulk electric resistance is known from the materials data sheets, and the BP–GDL contact resistance can be determined experimentally [24,28], the MEA resistivity can be calculated as:

$$R_{mem} = HFR - R_{BP} - R_{GDL} - 2R_c \quad (1)$$

Results for the cell under analysis were reported in [24].

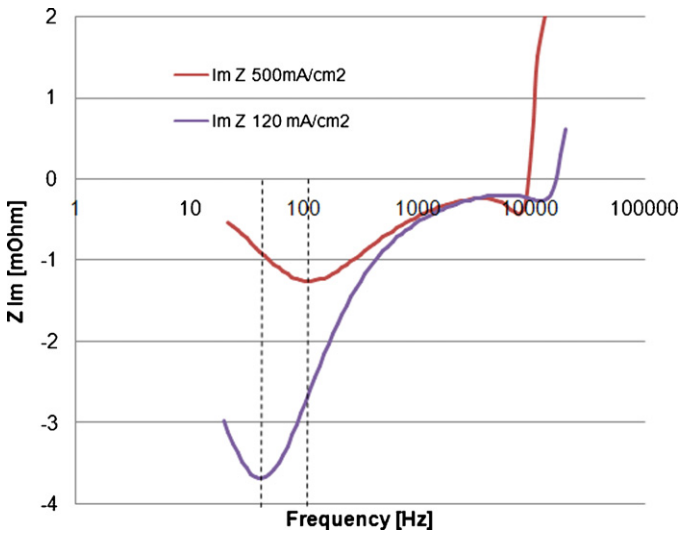

Fig. 4. Bode diagram corresponding to an operation with H_2/O_2 and RH = 100%. AC frequency range 20 Hz to 20 kHz.

4. Discussion and application to the non-dimensional analysis of fuel cell phenomena

4.1. Electrochemical and GDL diffusion mass transport time scales: Damkhöler number

The results plotted in the Nyquist diagram can also be interpreted as characteristic time scales of the different processes occurring within the fuel cell. The time constant τ of a particular physical or chemical phenomenon corresponds to the frequency peak of the corresponding arc in the Nyquist plot. Therefore, $\tau = 1/f_{peak}$ [29]. As frequency is not explicitly shown in Nyquist plots, the representation of the impedance versus frequency in a Bode diagram is more convenient.

By determining the time constants of the different processes a non-dimensional analysis can be derived. In particular, a fuel cell Damkhöler number can be used so that:

$$\mathrm{Da_{PEMFC}} = \frac{\text{EC reaction rate}}{\text{MT rate}} \tag{2}$$

$$\mathrm{Da_{PEMFC}} = \frac{\tau_{diff}}{\tau_{EC}} \tag{3}$$

The electrochemical reaction rate (EC reaction rate) corresponds to the rate of the oxygen oxidation reaction (ORR) as it is the limiting reaction in most cases [5,30]. The mass transport rate (MT rate) is assumed to be controlled by oxygen reactant diffusion in the GDL. The derivation of the time constants and the related Damkhöler numbers are presented in the following sections.

4.1.1. Electrochemical time scales

Fig. 4 shows the Bode diagrams for 120 and 500 mA cm^{-2} for the cell operating with H_2/O_2 and full humidification, where the corresponding Nyquist plot was shown in Fig. 3. The imaginary component of the impedance is represented versus the frequency. The peaks of the impedance values correspond to the maximum values of imaginary impedance in the Nyquist plots, and from the frequencies featuring such peak impedances the time constants can be derived. The time constants for the ORR (dashed lines) are calculated according to $\tau = 1/f_{peak}$ [29], so that τ_{EC} can be obtained from the Bode diagrams. As shown in Fig. 4, the enhanced driving force for the electrochemical reaction at larger current densities is involving a minor time constant: 9.0 ms for 500 mA cm^{-2} and 25.0 ms para 120 mA cm^{-2}.

4.1.2. GDL diffusion mass transport time scales

The value of τ_{diff} can be obtained in the same manner from Nyquist/Bode diagrams representing the low frequency arc in the frequency range 0.1–10 Hz [1,19]. Alternatively, different approximations can be used, such as [31]:

$$\tau_{diff} = \frac{\delta_{GDL}^2}{D_{eff}} \tag{4}$$

where δ_{GDL} is the GDL thickness and D_{eff} is the oxygen effective diffusion coefficient. τ_{diff} represents the diffusion time or characteristic time scale of diffusion, which is the time for significant diffusion to reach a given distance δ [32].

In order to determine D_{eff}, the standard diffusion coefficient must be corrected with the GDL porosity and the degree of flooding by liquid water pore blockage, where the correlation from Nam and Kaviany [33] has been used in the present analysis. Additionally, temperature and pressure effects must be also considered as stated in the work by Um et al. [34]. Considering all the effects affecting the effective diffusivity of reactants through the GDL, D_{eff} is calculated as:

$$D_{eff} = D_0 \left(\frac{\varepsilon - 0.11}{1 - 0.11}\right)^{0.785} (1-s)^2 \left(\frac{P_0}{P}\right) \left(\frac{T}{T_0}\right)^{1.5} \tag{5}$$

where T_0, P_0 are the reference temperature and pressure, 300 K and 101,325 Pa, and s is the water saturation (volume fraction of liquid water). The terms correcting D_0 are $\left(\frac{\varepsilon-0.11}{1-0.11}\right)^{0.785}$, corresponding to the correction for the GDL porosity and degree of flooding (according to the work of Nam and Kaviany [33] for details), and $\left(\frac{P_0}{P}\right)\left(\frac{T}{T_0}\right)^{1.5}$, corresponding to the correction for temperature and pressure according to Um et al. [34].

Another well established model for describing the effective diffusivity in GDL porous media proposes that:

$$D_{eff} = D_0 \varepsilon^{1.5} \tag{6}$$

where the exponent 1.5 is used in order to account for the medium tortuosity. This is known as the Bruggeman correction (the original work was published by Bruggeman [35]), and the approach is commonly used in fuel cell modelling [36–38].

Both Eqs. (5) and (6) yield similar results for the high porosities typically used in the GDL. For the cell under analysis described in Section 2.1, with $\varepsilon = 0.82$ [39], differences in the D_{eff} values are less than 8% when calculated according to Eqs. (5) and (6).

With a GDL porosity $\varepsilon = 0.82$, an oxygen diffusivity in air $D_{0,O_2-air} = 1.88E-5$ m^2 s^{-1} (average between the value reported in transport properties tables [40] and the value resulting from the Fuller–Schettler–Giddings equation), and considering the cell operating conditions (4 bar, 60° C), the value calculated using Eq. (5) for $D_{eff\text{-}Air}$ is 4.6E−6 m^2 s^{-1}, which is 25% of the standard oxygen diffusivity value in air. For the case operating with oxygen, $D_{0,O_2-H_2O} = 2.27E-5$ m^2 s^{-1} according to the Fuller–Schettler–Giddings equation, and considering the cell operating conditions the value calculated for D_{eff,O_2} is 5.56E−6 m^2 s^{-1}. The water saturation value has been considered to be zero at the current densities and cell conditions under analysis. This is because even at the highest current density in Fig. 3 (500 mA cm^{-2}), no concentration polarization effects are still observed in the polarization curve (Fig. 5). The calculated values of τ_{diff} (Eq. (4)) are 38 ms for air and 32 ms for oxygen.

For hydrogen, $D_{0,H_2-H_2O} = 8.16E-5$ m^2 s^{-1} (average between the value reported in transport properties tables [18] and the value resulting from the Fuller–Schettler–Giddings equation), and considering the cell operating conditions (4 bar, 60° C), the value calculated for $D_{eff\text{-}H_2} = 2.0E-5$ m^2 s^{-1}.

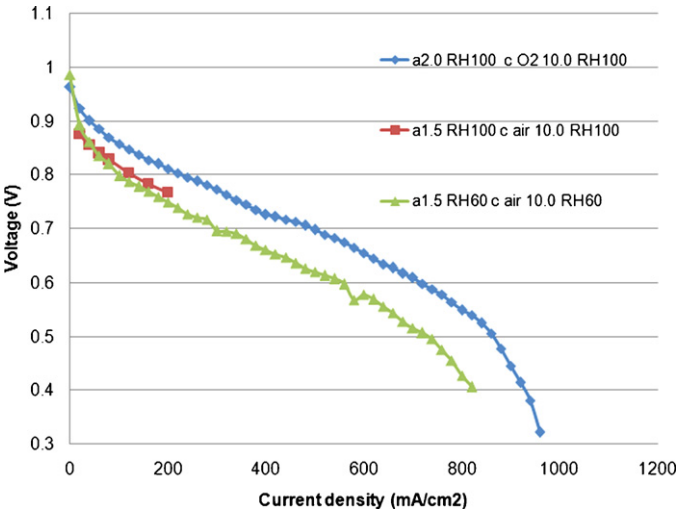

Fig. 5. Polarization curves of the cell analysed.

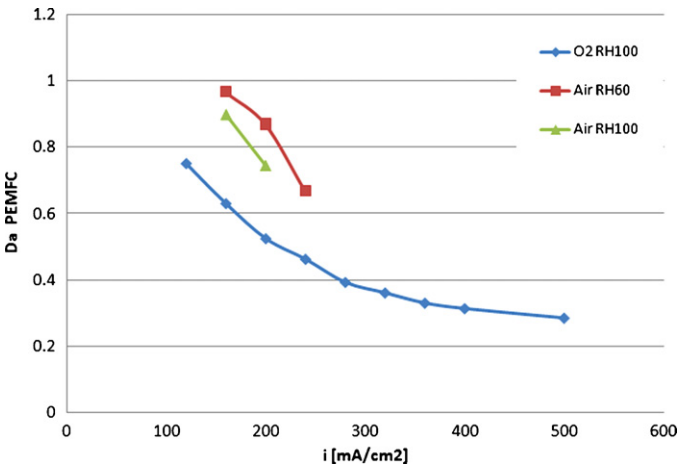

Fig. 6. Electrochemical characteristic times for operation with air and oxygen.

4.1.3. Damkhöler numbers

The characteristic time scales for the electrochemical reaction rate and the reactant diffusion in the GDL, as calculated in the previous sections, are reported in Table 2. The resulting Damkhöler numbers are also presented in Fig. 6. The results indicate that the reactant diffusion in the GDL is the limiting process for the cases considered, especially when oxygen is used as reactant at higher current densities. This result is obtained even at low current densities (160 mA cm^{-2}) indicating a non-balanced design of the electrode and GDL for this cell, which is probably a consequence of the selection of cell components from different suppliers (described in Section 2.1).

The balance between electrochemical reaction and diffusive mass transport can be further analysed as follows. In the steady-state operation, the reactant diffusive mass transport equals the reactant consumption via the electrochemical reaction. The oxygen consumption at the electrode is:

$$S_{O_2} = -\left(\frac{M_{w,O_2}}{4F}\right) R_{cat} \tag{7}$$

where R_{cat} is the cathode volumetric transfer current given by the Butler–Volmer equation, M_{w,O_2} is the oxygen molecular weight, and F is the Faraday constant. The diffusive flux from the GDL to the electrochemical active surface area is defined by:

$$J_{O_2} = \frac{\rho D_{eff-O_2}}{\delta_{GDL}} (y_{O_2,GDL} - y_{O_2,S}) \tag{8}$$

where ρ is the density, $y_{O_2,GDL}$ and $y_{O_2,S}$ is the oxygen mass fraction at GDL and reaction sites respectively. The volumetric consumption of oxygen S_{O_2} can be transformed into a surface flux by dividing its value by the specific surface area of the catalyst or surface-to-volume ratio (a). In steady state operation, both processes are balanced while one of them is limiting the overall rate of the process. The balance can be written by combining Eqs. (7) and (8):

$$\frac{\rho D_{eff-O_2}}{\delta_{GDL}} (y_{O_2,GDL} - y_{O_2,S}) = \frac{1}{a}\left(\frac{M_{w,O_2}}{4F}\right) R_{cat} \tag{9}$$

For the cases analysed, the limiting term in Eq. (9) is the GDL diffusive mass transport as demonstrated by the corresponding Damkhöler numbers.

4.2. Channel and GDL mass transport time scales

Channel design must ensure an appropriate reactant distribution over the electrode. Given the typical channel dimensions and reactants mass flows, the flow regime is always laminar, so that the convective mass transport is represented by the Sherwood number [41]:

$$Sh_{ch} = \frac{hd}{ch} \sim 2.6 \tag{10}$$

where h is the convective mass transfer coefficient for channel-GDL, d is the channel depth, and D_{ch} is the diffusion coefficient. The characteristic time scale for the reactant convective mass transport is therefore d/h, or:

$$\tau_{chMT} = \frac{d}{h} \sim \frac{d^2}{2.6 D_{ch}} \tag{11}$$

For the channel depth of the bipolar plate shown in Fig. 1 (d = 0.0011 m), τ_{chMT} = 20 ms for O_2, 25 ms for air, and 57 ms for H_2.

By combining Eqs. (4) and (11) a characteristic time scales ratio for the reactant transport in channels (convective) and GDL (diffusive) can be obtained:

$$\frac{\tau_{chMT}}{\tau_{diff}} = \frac{d^2 \delta_{GDL}^2}{2.6 D_{ch} D_{eff}} \tag{12}$$

Table 2
Electrochemical reaction characteristic time scale, Damkhöler numbers, and flow residence times. δ_{GDL} = 0.42 mm, $D_{eff-air}$ = 4.6E−6 m^2 s^{-1}, D_{eff-O_2} = 5.56E − 6 m^2 s^{-1}, $\tau_{diff-air}$ = 38 ms, D_{diff-O_2} = 32 ms, τ_{chMT} = 20 ms for O_2, 25 ms for air, and 57 ms for H_2.

λ_a	RH_a (%)	λ_c	RH_c (%)	Oxidant	i (mA cm^{-2})	τ_{EC} (s)	Da_{PEMFC}	τ_{chrt}, a (s)	τ_{chrt}, c (s)
1.5	60	5.0	60	Air	160	0.033	0.87	1.939	0.243
1.5	100	5.0	100	Air	160	0.028	0.74	1.939	0.243
2.0	100	10.0	100	Oxygen	120	0.025	0.75	1.939	0.774
2.0	100	10.0	100	Oxygen	160	0.020	0.63	1.454	0.581
2.0	100	10.0	100	Oxygen	200	0.016	0.52	1.163	0.465
2.0	100	10.0	100	Oxygen	400	0.010	0.21	0.582	0.232
2.0	100	10.0	100	Oxygen	500	0.009	0.28	0.465	0.186

A combined design of both channel and GDL should ensure that $\tau_{chMT}/\tau_{diff} \sim 1$, so that no limiting process is controlling the mass transfer rate. However, it is widely known that in general $\tau_{chMT} < \tau_{diff}$ given the GDL characteristics in terms of porosity and water management, especially at high current densities. For the cases considered, $\tau_{chMT}/\tau_{diff} = 0.65$, indicating a mass transfer process controlled by the diffusive mass transport in the GDL.

In the same manner, the flow residence time in the channel must ensure that the convection mass transport occurs, thus the flow residence time must be larger than the convective mass transport time scale:

$$\tau_{chrt} > \tau_{chMT} \tag{13}$$

where $\tau_{chrt} = L/V$. For the bipolar plate considered, $L = 0.63$ m. The flow velocity V depends on the channel cross-section ($0.78\,\text{mm} \times 1.1\,\text{mm}$) and the volume flow, which depends on the current density and stoichiometric factor:

$$Q_{v,H_2} = 6.97 I \lambda_a \tag{14}$$

$$Q_{v,O_2} = 3.49 I \lambda_c \tag{15}$$

$$Q_{v,Air} = 16.7 I \lambda_c \tag{16}$$

where I is the current intensity (A) and λ the stoichiometric factor. For the cell under analysis with five path-serpentine flow field design, the total Q_v is split into the five parallel channels in order to analyse a single channel. Table 2 lists the τ_{chrt} values obtained for this analysis for the anode and cathode sides. The comparison between τ_{chrt} values against τ_{chMT} values shows that the residence times of anode and cathode flows are long enough in order to assure the appropriate mass transfer process to the GDL for all cases considered in the analysis.

5. Conclusions

AC impedance results for a 50 cm^2 PEM fuel cell are presented. Besides analyzing the electrode charge transfer resistance from the Nyquist plots obtained for different operating conditions, this work outlines a non-dimensional analysis of PEM fuel cell transport phenomena. Characteristic time scales for electrochemical reaction and reactant transport processes in channels and GDL are derived either from experimental Bode plots or from correlations found in the literature. Damkhöler numbers were calculated for a range of operating conditions, which can help understanding and quantifying the fundamental processes limiting the performance of a PEM fuel cell. Characteristic times for channel-GDL convective mass transfer and GDL bulk diffusive mass transfer was also compared, and the appropriateness of the channel design in terms of flow residence time was studied. For the cell and operating conditions analysed, the investigation shows that diffusion in GDL is constantly the limiting transport process even at low current densities (160 mA cm^{-2}) indicating a non-balanced design of the electrode and GDL for this cell, which is probably a consequence of the selection of cell components from different suppliers. Additional measurements in the low frequency range (0.1–10 Hz) are needed in order to allow for additional experimental analysis, which will provide further information about the mass transport phenomena also necessary for the validation of the non-dimensional analysis presented in this work.

Acknowledgements

This work has been funded by the Secretariat-General of Universities, Research and Technology, from Junta de Andalucía, under the P08-TEP-4309 project. Authors also acknowledge INTA for its close collaboration in PEMFC CFD modelling and experimental validation.

References

[1] X. Yuan, H. Wang, J.C. Sun, J. Zhang, Int. J. Hydrogen Energy 32 (2007) 4365–4380.
[2] J. Wu, X.Z. Yuan, H. Wang, M. Blanco, J.J. Martin, J. Zhang, Int. J. Hydrogen Energy 33 (2008) 1735–1746.
[3] A. Parthasarathy, B. Davé, S. Srinivasan, J. Appleby, C. Martin, J. Electrochem. Soc. 139 (1992) 1634–1641.
[4] O. Antoine, Y. Bultel, R. Durand, J. Electroanal. Chem. 499 (2001) 85–94.
[5] K.C. Neyerlin, W. Gu, J. Jorne, H.A. Gasteiger, J. Electrochem. Soc. 153 (2006) A1955–A1963.
[6] H. Xu, Y. Song, H.R. Kunz, J.M. Fenton, J. Electrochem. Soc. 152 (2005) A1828–A1836.
[7] K.C. Neyerlin, H.A. Gasteiger, C.K. Mittelsteadt, J. Jorne, W. Gu, J. Electrochem. Soc. 152 (2005) A1073–A1080.
[8] N. Wagner, E. Gülzow, J. Power Sources 127 (2004) 341–347.
[9] T.E. Springer, T.A. Zawodzinski, M.S. Wilson, S. Gottesfeld, J. Electrochem. Soc. 143 (1996) 587–599.
[10] M. Eikerling, A.A. Kornyshev, J. Electroanal. Chem. 475 (1999) 107–123.
[11] M.C. Lefebvre, R.B. Martin, P.G. Pickup, Electrochem. Solid-State Lett. 2 (1999) 259–261.
[12] A.P. Saab, F.H. Garzon, T.A. Zawodzinski, J. Electrochem. Soc. 149 (2002) A1541–A1546.
[13] A.P. Saab, F.H. Garzon, T.A. Zawodzinski, J. Electrochem. Soc. 150 (2003) A214–A218.
[14] Y. Liu, M.W. Murphy, D.B. Baker, W. Gu, C. Ji, J. Jorne, H.A. Gasteiger, J. Electrochem. Soc. 156 (2009) B970–B980.
[15] K.R. Cooper, M. Smith, J. Power Sources 160 (2006) 1088–1095.
[16] T. Romero-Castañón, L.G. Arriaga, U. Cano-Castillo, J. Power Sources 118 (2003) 179–182.
[17] J.M. Song, S.Y. Cha, W.M. Lee, J. Power Sources 94 (2001) 78–84.
[18] N. Wagner, J. Appl. Electrochem. 32 (2002) 859–863.
[19] N. Fouquet, C. Doulet, C. Nouillant, G. Dauphin-Tanguy, B. Ould-Bouamama, J. Power Sources 159 (2006) 905–913.
[20] W. Meïrida, D.A. Harrington, J.M. Le Canut, G. McLean, J. Power Sources 161 (2006) 264–274.
[21] A. Hakenjos, M. Zobel, J. Clausnitzer, C. Hebling, J. Power Sources 154 (2006) 360–363.
[22] E.L. Gyenge, J. Power Sources 152 (2005) 105–121.
[23] S. Shimpalee, M. Ohashi, J.W. Van Zee, C. Ziegler, C. Stoeckmann, C. Sadeler, C. Hebling, Electrochim. Acta 54 (2009) 2899–2911.
[24] A. Iranzo, M. Muñoz, J. Pino, F. Rosa, Int. J. Hydrogen Energy 35 (2010) 11437–11447.
[25] A. Iranzo, M. Muñoz, F. Rosa, J. Pino, Int. J. Hydrogen Energy 35 (2010) 11533–11550.
[26] The fuel cell testing and standarization network. EU FP5 Project ENG2-CT-2002-20657 FCTESTNET test procedures draft v1.4, 2006.
[27] M. Mench, Fuel Cell Engines, first ed., Wiley, New Jersey, 2008, pp. 454–458.
[28] F. Barbir, PEM Fuel Cells: Theory and Practice, first ed., Elsevier Academic, Amsterdam/London, 2005, 254–258.
[29] E. Ivers-Tiffée, A. Weber, H. Schichlein, in: W. Vieltisch, A. Lamm, H.A. Gasteiger (Eds.), Handbook of Fuel Cells, John Wiley, Chichester, UK, 2003, pp. 220–235.
[30] H.A. Gasteiger, S.S. Kocha, B. Sompalli, F.T. Wagner, Appl. Catal. B: Environ. 56 (2005) 9–35.
[31] C.Y. Wang, Chem. Rev. 104 (2004) 4727–4765.
[32] E.L. Cussler, Diffusion-Mass Transfer in Fluid Systems, second ed., Cambridge University Press, New York, 1997, pp. 101.
[33] J.H. Nam, M. Kaviany, Int. J. Heat Mass Transfer 46 (2003) 4595–4611.
[34] S. Um, C.Y. Wang, K.S. Chen, J. Electrochem. Soc. 147 (2000) 4485–4493.
[35] D.A.G. Bruggeman, Ann. Phys. 416 (1935) 636–664.
[36] P.T. Nguyen, T. Berning, N. Djilali, J. Power Sources 130 (2004) 149–157.
[37] X.D. Wang, Y.Y. Duan, W.M. Yan, X.F. Peng, J. Power Sources 175 (2008) 397–407.
[38] W. Sun, B.A. Peppley, K. Karan, J. Power Sources 144 (2005) 42–53.
[39] SGL Group, http://www.sglgroup.com/cms/international/products/product-groups/su/fuel-cell-components/, 2009.
[40] P.E. Liley, R.C. Reid, E. Buck, in: R.H. Perry, D. Green (Eds.), Perry's Chemical Engineers Handbook, McGraw-Hill, New York, 1984, pp. 3.256–3.257.
[41] R.N. Carter, W. Gu, B. Brady, P.T. Yu, K. Subramanian, H.A. Gasteiger, in: A. Lamm, W. Vieltisch, H.A. Gasteiger (Eds.), Handbook of Fuel Cells, John Wiley, Chichester, UK, 2009, pp. 829–843.